

Published in final edited form as:

J Phys Chem C Nanomater Interfaces. 2009 November 12; 113(45): 19609–19617. doi:10.1021/jp906367t.

Tripodal Binding Units for Self-Assembled Monolayers on Gold: A Comparison of Thiol and Thioether Headgroups

Tobias Weidner^{1,*}, Nirmalya Ballav^{2,#}, Ulrich Siemeling³, Dennis Troegel⁴, Tim Walter⁴, Reinhold Tacke^{4,*}, David G. Castner¹, and Michael Zharnikov^{2,*}

¹ National ESCA and Surface Analysis Center for Biomedical Problems (NESAC/BIO), Departments of Bioengineering and Chemical Engineering, University of Washington, Seattle, WA 98195, USA

² Angewandte Physikalische Chemie, Universität Heidelberg, 69120 Heidelberg, Germany

³ Institut für Chemie and Center for Interdisciplinary Nanostructure Science and Technology (CINaT), Universität Kassel, 34109 Kassel, Germany

⁴ Institut für Anorganische Chemie, Universität Würzburg, Am Hubland, 97074 Würzburg, Germany

Abstract

Whereas thiols and thioethers are frequently used as binding units of oligodentate precursor molecules to fabricate self-assembled monolayers (SAMs) on coinage metal and semiconductor surfaces, their use for tridentate bonding configuration is still questionable. Against this background, novel tridentate thiol ligands, PhSi(CH₂SH)₃ (**PTT**) and *p*-Ph-C₆H₄Si(CH₂SH)₃ (**BPTT**), were synthesized and used as tripodal adsorbate molecules for the fabrication of SAMs on Au(111). These SAMs were characterized by X-ray photoelectron spectroscopy (XPS) and near edge X-ray absorption fine structure (NEXAFS) spectroscopy. The **PTT** and **BPTT** films were compared with the analogous systems comprised of same tripodal ligands with thioether instead of thiol binding units (anchors). XPS and NEXAFS data suggest that the binding uniformity, packing density, and molecular alignment of the thiol-based ligands in the respective SAMs is superior to their thioether counterparts. In addition, the thiol-based films showed significantly lower levels of contamination. Significantly, the quality of the **PTT** SAMs on Au(111) was found to be even higher than that of the films formed from the respective monodentate counterpart, benzenethiol. The results obtained allow for making some general conclusions on the specific character of molecular self-assembly in the case of tridentate ligands.

1. Introduction

Controlling the properties of surfaces and interfaces is one of the most important challenges for the scientific and industrial communities. Self-assembled monolayers (SAMs), which are 2D polycrystalline monomolecular films attached to suitable substrates, can meet this demand to a large extent, because the tail group of the SAM represents a new surface with a

* Authors to whom correspondence should be addressed: M. Z.; phone: +49-6221-54 4921; fax: +49-6221-54 6199; Michael.Zharnikov@urz.uni-heidelberg.de; T. W.; phone: +1-206-685-0452; fax: +1-206-543-3778; weidner@nb.engr.washington.edu; R. T.; phone: +49-931-31-85250; fax: +49-931-888-4609; r.tacke@uni-wuerzburg.de.
 #Present address: Laboratory for Micro and Nanotechnology, Paul Scherrer Institut, 5232 Villigen, Switzerland

Supporting Information Available

The results of NMR-spectroscopic characterization and elemental analyses of 1a, 1b, 2a, 2b, PTT, and BPTT are presented in the Supporting Information, along with selected crystallographic data for BPTT. This information is available free of charge via the Internet at <http://pubs.acs.org>.

chemical and physical identity that is redefined, to a large extent, by the tail group functional properties.¹⁻⁴ Molecules capable of spontaneous formation of SAMs consist usually of three basic building blocks: a headgroup for strong and stable attachment to the substrate, a functional group that is exposed at the SAM–ambient interface (tail group), and a spacer chain that separates the head- and tail groups and drives the self-assembly by lateral interactions between adjacent molecules. SAMs are frequently used to tailor the surface chemistry and physical properties for applications in such diverse fields as, e.g., molecular electronics,⁵ chemical vapor sensing,^{6,7} as well as bio-^{8,9} and nanotechnology.¹⁰ Another promising application is the preparation of smart surfaces decorated with, e.g., molecular switches,¹¹⁻¹⁴ chemical or magnetic data storage,¹⁵ and molecular machines^{16,17} (also light-powered)^{11,18,19} using complex functional tail groups. However, these functional units are often sterically demanding and - due to their dimensions, polarity, and/or chemical reactivity - tend to disturb the lateral intermolecular interaction responsible for SAM ordering. This can result in severe deterioration of the film quality. Mixed two-component monolayers have been used to avoid this problem with some success, but phase segregation and the burying of functional, terminal units within the film are still unresolved issues for most systems. An alternative and increasingly popular single-component strategy is the use of binding units (i.e. headgroups), which cover a surface area comparable or even exceeding the lateral dimensions of the functional unit.^{20,21} In this regard, ligands with multiple attachment points have been widely used. Since a plane is defined by three points, the most straightforward approach was based on adsorbate molecules with three binding groups,²²⁻²⁵ although four,²⁶⁻²⁹ or more^{30,31} anchors have also been realized and used to immobilize large functional groups such as, e.g., ferrocene³²⁻³⁸ and switchable groups like photo-responsive azobenzene units, which require a considerable amount of free space for unhindered isomerization.³⁹⁻⁴¹ Owing to a “surface chelate” effect, oligodentate adsorbate molecules are expected to bind particularly strongly to the substrate.^{42,43} Thiol^{22-25,30,31} and thioether²⁶⁻²⁹ moieties are currently the most widely used binding units in this context, since they provide efficient coupling of the ligands to a variety of different metal and semiconductor substrates. However, the use of thioethers generally leads to films of inferior stability since their interaction with a gold substrate is weaker and the respective bond less stable as compared with the corresponding thiol functionality.⁴⁴ On the other hand, thioethers are assumed to be more mobile on the surface, which could be important for lateral diffusion during self-assembly, to avoid the formation of incomplete monolayers (also referred to as “car parking problem”).

Both types of chemistry have been extensively used for monolayer formation, but a systematic comparison of the quality of thiol- and thioether-based tripod ligand SAMs has not yet been performed.

Recently, we have described the properties of monomolecular films formed on gold surfaces from the tripodal adsorbate species $\text{PhSi}(\text{CH}_2\text{SMe})_3$ (**PTET**) and $p\text{-Ph-C}_6\text{H}_4\text{Si}(\text{CH}_2\text{SMe})_3$ (**BPTET**), which contain a tridentate thioether headgroup (see Scheme 1).⁴⁵ According to high-resolution X-ray photoelectron spectroscopy (XPS) data, uniform attachment of the tridentate moieties to the substrate does not occur in the case of these compounds. Three different bonding configurations, including thiolate-type and coordination-type anchors were observed, and the packing density of the resulting films was quite low. These results were not fully satisfactory, so that a further development was necessary. In view of this general goal, we report here the properties of more advanced systems, viz. the SAMs fabricated from the novel tripodal thiols $\text{PhSi}(\text{CH}_2\text{SH})_3$ (**PTT**) and $p\text{-Ph-C}_6\text{H}_4\text{Si}(\text{CH}_2\text{SH})_3$ (**BPTT**) and compare these systems with the **PTET** and **BPTET** films. The thiol-based tripod ligands are shown in Scheme 1.

The following section describes the preparative approach and experimental techniques. The results are presented and preliminarily discussed in Section 3. A more extensive discussion of the data is given in Section 4, followed by a summary in Section 5.

2. Experimental Section

2.1 Syntheses

All syntheses were carried out under dry nitrogen. The organic solvents used were dried and purified according to standard procedures and stored under dry nitrogen.

Trichloro(phenyl)silane was commercially available, and (4-biphenyl)trichlorosilane was prepared according to a literature procedure.⁴⁵ Chemicals were purchased from Aldrich and Acros and used as received without further purification. A Büchi GKR-51 apparatus was used for the bulb-to-bulb distillations. Melting points were determined with a Büchi Melting Point B-540 apparatus using samples in sealed glass capillaries.

Tris(chloromethyl)phenylsilane (1a)—A 2.5 M solution of *n*-butyllithium in hexanes (109 mL, 273 mmol of *n*-BuLi) was added dropwise at $-70\text{ }^{\circ}\text{C}$ ($\pm 5\text{ }^{\circ}\text{C}$, temperature measurement within the flask) within 6 h to a stirred mixture of trichloro(phenyl)silane (19.1 g, 90.3 mmol), bromochloromethane (52.8 g, 408 mmol), and tetrahydrofuran (160 mL) (the *n*-butyllithium solution was added via a special horizontally elongated side neck of the three-necked flask, which itself was immersed in the cooling bath to ensure pre-cooling of the *n*-butyllithium solution before making contact with the reaction mixture). After the addition was complete, the mixture was warmed to $20\text{ }^{\circ}\text{C}$ within 16 h. The solvent was removed under reduced pressure, water (200 mL) and diethyl ether (200 mL) were added, the organic phase was separated, and the aqueous phase was extracted with diethyl ether ($2 \times 400\text{ mL}$). The combined organic extracts were dried over anhydrous sodium sulfate, the solvent was removed under reduced pressure, and the resulting residue was purified by bulb-to-bulb distillation (oven temperature $105\text{--}110\text{ }^{\circ}\text{C}$, 0.1 mbar) to give **1a** in 83% yield as a colorless liquid (19.0 g, 74.9 mmol).

(4-Biphenyl)tris(chloromethyl)silane (1b)—A 2.5 M solution of *n*-butyllithium in hexanes (35 mL, 87.5 mmol of *n*-BuLi) was added dropwise at $-70\text{ }^{\circ}\text{C}$ ($\pm 5\text{ }^{\circ}\text{C}$, temperature measurement within the flask) within 4 h to a stirred mixture of (4-biphenyl)trichlorosilane (8.30 g, 28.9 mmol), bromochloromethane (16.8 g, 129.8 mmol), and tetrahydrofuran (50 mL) (the *n*-butyllithium solution was added via a special horizontally elongated side neck of the three-necked flask, which itself was immersed in the cooling bath to ensure pre-cooling of the *n*-butyllithium solution before making contact with the reaction mixture). After the addition was complete, the mixture was warmed to $20\text{ }^{\circ}\text{C}$ within 16 h. The solvent was removed under reduced pressure, water (200 mL) and diethyl ether (200 mL) were added, the organic phase was separated, and the aqueous phase was extracted with diethyl ether ($2 \times 200\text{ mL}$). The combined organic extracts were dried over anhydrous sodium sulfate, the solvent was removed under reduced pressure, and the residue was purified by column chromatography on silica gel (silica gel, $32\text{--}63\text{ }\mu\text{m}$ (ICN 02826); eluent, *n*-hexane/ethyl acetate (19:1 (v/v)). The relevant fractions (GC control) were combined, and the solvent was removed under reduced pressure to give **1b** in 53% yield as a colorless solid (5.08 g, 15.4 mmol); mp $47\text{--}48\text{ }^{\circ}\text{C}$.

Tris(acetylthiomethyl)phenylsilane (2a)—Compound **1a** (9.50 g, 37.5 mmol) was added in a single portion at $20\text{ }^{\circ}\text{C}$ to a stirred suspension of potassium thioacetate (19.4 g, 170 mmol) in tetrahydrofuran (500 mL), and the resulting mixture was stirred at $20\text{ }^{\circ}\text{C}$ for 22 h. The solvent was removed under reduced pressure, diethyl ether (250 mL) and water (160 mL) were added, and the aqueous phase was extracted with diethyl ether ($2 \times 150\text{ mL}$).

The combined organic extracts were dried over anhydrous sodium sulfate, the solvent was removed under reduced pressure, and the residue was purified by bulb-to-bulb distillation (oven temperature 245 °C, 0.7 mbar) to give **2a** in 86% yield as a yellowish liquid (12.0 g, 32.2 mmol).

Tris(acetylthiomethyl)(4-biphenyl)silane (2b)—Compound **1b** (4.00 g, 12.1 mmol) was added in a single portion at 20 °C to a stirred suspension of potassium thioacetate (7.10 g, 62.2 mmol) in tetrahydrofuran (180 mL), and the resulting mixture was stirred at 20 °C for 19 h. The solvent was removed under reduced pressure, diethyl ether (90 mL) and water (60 mL) were added, and the aqueous phase was extracted with diethyl ether (2 × 50 mL). The combined organic extracts were dried over anhydrous sodium sulfate, the solvent was removed under reduced pressure, and the residue was purified by column chromatography on silica gel (silica gel, 32–63 μm (ICN 02826); eluent, *n*-hexane/ethyl acetate (6:1 (v/v)) to give **2b** in 78% yield as a yellowish liquid (4.24 g, 9.45 mmol).

Tris(mercaptomethyl)phenylsilane (PTT)—A solution of **2a** (12.0 g, 32.2 mmol) in diethyl ether (159 mL) was added dropwise at 0 °C within 100 min to a stirred suspension of lithium aluminum hydride (9.14 g, 241 mmol) in diethyl ether (300 mL), and the resulting mixture was stirred at 0 °C for 2 h and then at 20 °C for a further 18 h. Subsequently, hydrochloric acid (1 M, 180 mL) was added dropwise at 0 °C within 90 min under stirring, and the resulting mixture was then warmed to 20 °C. Water (800 mL) and diethyl ether (550 mL) were added, the organic phase was separated, and the aqueous phase was extracted with diethyl ether (2 × 400 mL). The combined organic extracts were dried over anhydrous sodium sulfate, the solvent was removed under reduced pressure, and the residue was purified by bulb-to-bulb distillation (oven temperature 150 °C, 0.4 mbar) to give **PTT** in 79% yield as a colorless liquid (6.29 g, 25.5 mmol).

(4-Biphenyl)tris(mercaptomethyl)silane (BPTT)—A solution of **2b** (4.00 g, 8.91 mmol) in diethyl ether (40 mL) was added dropwise at 0 °C within 90 min to a stirred suspension of lithium aluminum hydride (4.03 g, 106 mmol) in diethyl ether (80 mL), and the resulting mixture was stirred at 0 °C for 2 h and then at 20 °C for a further 14 h. Subsequently, hydrochloric acid (2 M, 75 mL) was added dropwise at 0 °C within 2 h under stirring, and the resulting mixture was then warmed to 20 °C. Water (275 mL) and diethyl ether (180 mL) were added, the organic phase was separated, and the aqueous phase was extracted with diethyl ether (2 × 150 mL). The combined organic extracts were dried over anhydrous sodium sulfate, the solvent was removed under reduced pressure, and the residue was crystallized from boiling *n*-hexane/diethyl ether (20:9 (v/v)) (58 mL; slow cooling to –20 °C and crystallization over a period of 24 h). The product was isolated by filtration, washed with cold (0 °C) *n*-hexane (20 mL), and dried in vacuo (10 mbar, 20 °C, 2 h) to give **BPTT** in 61% yield (including the workup of the mother liquor) as a colorless crystalline solid (1.76 g, 5.46 mmol); mp 39 °C.

2.2 Crystal structure analysis

(4-Biphenyl)tris(mercaptomethyl)silane (**BPTT**) was structurally characterized by single-crystal X-ray diffraction: A suitable single crystal was mounted in inert oil (perfluoropolyalkyl ether, ABCR) on a glass fiber and then transferred to the cold nitrogen gas stream of the diffractometer (Bruker Nonius KAPPA APEX II CCD system with Montel mirror; MoK_α radiation, λ = 0.71073 Å). The structure was solved by direct methods (SHELXS-97) and refined by full-matrix least-squares methods on *F*² for all unique reflections (SHELXL-97). For the CH hydrogen atoms, a riding model was employed. CCDC-XXXXXX contains the supplementary crystallographic data for this paper. These

data can be obtained free of charge from The Cambridge Crystallographic Data Centre via www.ccdc.cam.ac.uk/data_request/cif.

2.3 Film preparation

The gold substrates for the SAM fabrication were prepared by thermal evaporation of 100 nm gold (99.99% purity) onto polished single-crystal silicon (111) wafers (Silicon Sense) primed with a 5 nm titanium layer for adhesion promotion. The resulting films were polycrystalline with a grain size of 20–50 nm and predominantly possessed (111) orientation.⁴⁶ The films were formed by immersion of freshly prepared gold substrates in 10 μ M solutions of **PTT** and **BPTT**, respectively, in ethanol at room temperature for 18 h. After immersion, the samples were carefully rinsed with copious amounts of ethanol, blown dry with nitrogen, and then kept in plastic or glass containers filled with nitrogen until they were characterized.

In addition to the **PTT** and **BPTT** films, we have also prepared SAMs of the related monodentate ligand, biphenyl-4-thiol, *p*-Ph-C₆H₄SH (**BPT**, see Scheme 1). The same preparation procedure as for **PTT** and **BPTT** films was used. The **BPT** SAMs were used as a reference.

2.4 X-ray photoelectron spectroscopy

The **PTET**, **BPTET**, and **BPT** films were characterized by high-resolution XPS (HRXPS). The measurements were carried out at the D1011 beamline of the MAX-lab synchrotron radiation facility in Lund, Sweden. The spectra were recorded in normal emission geometry at photon energies (PEs) of 350 and 580 eV. The binding energy (BE) scale of every spectrum was individually calibrated using the Au 4f emission line of the underlying gold substrate at 83.95 eV. The energy resolution was better than 100 meV.

The **PTT** and **BPTT** films were characterized by XPS. These experiments were performed on a Kratos AXIS Ultra DLD instrument (Kratos, Manchester, England) in the hybrid mode using a monochromatic Al_{K α} X-ray source (PE=1486.6 eV) and normal emission geometry. The energy scale was calibrated to the Au 4f_{7/2} emission of the underlying gold substrate. The energy resolution was better than 400 meV.

All XPS and HRXPS spectra were fitted by symmetric Voigt functions and Shirley-type background. To fit the S 2p_{3/2,1/2} doublets, we used a branching ratio of 2 and a spin-orbit splitting (verified by fit) of 1.18 eV.⁴⁷ The fits were carried out self-consistently, i.e., the same parameters were used for identical spectral regions.

2.5 Near-edge X-ray absorption fine structure spectroscopy

NEXAFS measurements were performed at the HE-SGM beamline of the synchrotron storage ring BESSY II in Berlin, Germany. The spectra were collected at the C *K*-edge with a retardation voltage of -150 V. Linearly polarized light with a polarization factor of ~0.82 was used. The energy resolution was approximately 0.4 eV, and the incidence angle of the X-ray light was varied from 90° to 20° in 10–20° steps. Raw NEXAFS spectra were normalized to the incident photon flux by division through a spectrum of a clean, freshly sputtered gold sample. The photon energy scale was referenced to the prominent π_1^* resonance of freshly cleaved highly oriented pyrolytic graphite at 285.38 eV.⁴⁸ Further, the spectra were reduced to the standard form by subtracting linear pre-edge background and normalizing to the unity edge jump determined by a horizontal plateau 40–50 eV above the absorption edge.

3. Results

3.1 Synthesis and Characterization of PTT and BPTT

The synthesis of the tripodal thiols **PTT** (R = Ph) and **BPTT** (R = *p*-Ph-C₆H₄) is outlined in Scheme 2. Both compounds were prepared in three-step syntheses, starting from trichloro(phenyl)silane and (4-biphenyl)trichlorosilane, respectively. The synthetic strategy used for the preparation of **PTT** and **BPTT** is analogous to that for the synthesis of MeSi(CH₂SH)₃,⁴⁹ (TMOP)Si(CH₂SH)₃ (TMOP = 2,4,6-trimethoxyphenyl),⁵⁰ and Si(CH₂SH)₄.⁵¹ **PTT** was isolated as a colorless liquid (total yield: 56%), whereas **BPTT** was obtained as a colorless crystalline solid (total yield: 25%). The identities of both compounds were established by elemental analyses (C, H, S) and solution-state NMR spectroscopy (¹H, ¹³C, ²⁹Si) (for details, see Experimental Section and Supporting Information). In addition, **BPTT** was structurally characterized by single-crystal X-ray diffraction.

BPTT crystallizes in the space group $P\bar{1}$, with two molecules in the asymmetric unit. The structures of these two molecules are very similar and are shown in Figure 1. Selected geometric data for the C(Si(CH₂SH)₃) groups are given in the respective figure legend. The bond distances and angles are in the expected ranges and do not need any further discussion.

Not surprisingly, intermolecular S...S contacts of ca. 3.4 Å are observed between neighboring molecules in the crystal, which is below the sum of the estimated van der Waals radii (3.7 Å).⁵²⁻⁵³ The intricate nature of chalcogen...chalcogen interactions was recently analyzed by high-level quantum-chemical methods and is still a matter of current debate.⁵⁴⁻⁵⁶ It has been pointed out that, owing to the non-spherical electron density distribution around divalent sulfur, the effective size of divalent sulfur in S...S contacts is a function of the orientation of the substituents, with the shortest S...S contacts occurring when the substituents are coplanar. In this case, a lower limit of 2.9 Å has been rationalized for intramolecular contacts.⁵⁷⁻⁵⁹

3.2 X-Ray Photoelectron Spectroscopy

Normalized C 1s spectra of all the tripod ligand SAMs studied, along with a spectrum of a **BPT** film, are presented in Figure 2. The **BPT** SAM, consisting of monodentate ligands, served as a reference system since it has been well established that **BPT** forms well-defined high-fidelity monolayers on Au(111).⁶⁰⁻⁶⁴ The C 1s spectra of all tripod ligand SAMs exhibit a main emission near 284.5 eV related to the phenyl/4-biphenyl backbone of the film constituents. The respective BE is somewhat higher than that for the **BPT** film which can be presumably explained by electrostatic effects related to the different coupling between the phenyl/4-biphenyl backbones and the headgroups in the tripod ligand and **BPT** SAMs. The FWHM of the main C 1s emission is noticeably larger for the tripod ligand films than for the **BPT** SAM. This suggests a higher structural inhomogeneity in the former films, which had been observed for **PTET** and **BPTET** layers⁴⁵ and was expected to some extent for **PTT** and **BPTT** SAMs as well. No peaks related to oxygen-containing contaminations or oxidation of the molecular backbone are observed in the spectra of all studied films, except for the **PTET** SAM, which shows an intense emission from C–O species at around 286.0 eV and a weak feature near 288.8 eV related to carboxyl (C=O) or carboxylic acid (COOH) groups. Also, the FWHM of the main emission is exceptionally large for the latter film compared to the other SAMs studied here, which is an additional indication that the quality of this film is worse as compared to the other systems.

In addition to the above analysis of the C 1s spectra, the effective thickness of the SAMs was calculated within the standard theoretical framework, using reported attenuation

lengths.^{65,66} The obtained values of the effective thickness are summarized in Table 1 and are compared with theoretical estimates, which were calculated assuming an upright orientation of the molecules in the SAMs, based on the sum of the respective molecular lengths and the substrate–S bond length for the tridentate binding configurations. Note that the density of the tripod ligand films is probably significantly lower than in the densely packed alkanethiol films used as a reference. The effective thickness values discussed here therefore represent lower limits of the actual SAM thickness. For all 4-biphenyl-based systems (**BPT**, **PTT**, and **BPTET**), the derived thickness values are slightly lower than the respective theoretical estimates, which is understandable in view of possible molecular inclination and orientational disorder in the films. At the same time, the effective thicknesses of the **BPT** and **BPTT** SAMs are quite close to each other, suggesting a similar film quality, whereas the thickness value for **BPTET** is noticeably smaller.

In contrast to the 4-biphenyl-based systems (**BPTT**, **BPTET**, and **BPT**), the phenyl-based ones (**PTT** and **PTET**) show a larger film thickness than can be expected from the molecular structure, with much larger difference in the case of **PTET**. This difference could be related to the physisorbed molecular species at the SAM–ambient interface but most likely originates from contaminants, which were observed even in the case of analogous monodentate ligand binding,⁶⁴ and the presence of which is obvious in the case of the **PTET** film (see Figure 2). Note that contamination, which is always present on any surface exposed to ambient, is usually removed upon the formation of a densely packed SAM (so called self-cleaning) but persists to some extent if an effective assembly is hindered, e.g., by specific molecular architectures as in the case of **PTET**.

The XPS S 2p spectra of the tripod ligand and **BPT** SAMs are presented in Figure 3. The spectra of the former films exhibit several S 2p doublets at 161.0–161.2, 162.0, and 163.3–163.4 eV (S 2p_{3/2}); the relative intensities of these features are given in Table 2. No traces of oxidized sulfur species (higher BEs) are observed. A doublet near 162.0 eV is commonly assigned to a thiolate species, i.e., sulfur atoms strongly bound to the gold substrate.⁶⁷ This is the dominating emission in the spectrum of the **BPT** SAM, suggesting a predominantly thiolate-type attachment to the substrate for the vast majority of the **BPT** molecules. For the **PTET** and **BPTET** films, the relative intensity of the thiolate doublet is comparable to those of the features at 161.0 eV and 163.3 eV (S 2p_{3/2}), which implies a coexistence of different chemical states for the anchor groups in these SAMs. In contrast, the **PTT** and **BPTT** spectra do not exhibit a peak near 161.0 eV, but both spectra do exhibit significant doublets near 162.0 and 163.3 eV (S 2p_{3/2}). The presence of only a single binding sulfur species in the **PTT** and **BPTT** spectra suggests a more homogeneous bonding compared to the thioether tripod ligands. A doublet at 163.3–163.4 eV is commonly associated with weakly bound sulfur, unbound sulfur, or a disulfide moiety.^{67,68} In our case, the assignment of this doublet can be different for the thioether-based and thiol-based tripod systems. In the case of **PTET** and **BPTET**, this doublet can be assigned to a thioether making a weak coordination-type binding to the substrate, in line with previously reported studies, which show that thioethers can adsorb non-destructively on gold,^{68–71} although it has been shown that C–S bond cleavage can also occur,^{71,72} followed by a thiolate-like bonding to the substrate. In the case of **PTT** and **BPTT**, the doublet at 163.3–163.4 eV can be assigned to weakly coordinated or unbound thiol groups. The presence of this doublet in the spectra indicates that a fraction of the anchor groups is not bound to the gold substrate in the respective films.

The feature at 161.0 eV, which is quite pronounced in the spectra of **PTET** and **BPTET** films, can be ascribed either to atomic sulfur⁷³ or a thiolate-type bound sulfur with a different binding chemistry and/or geometry as compared to the “standard” thiolate-type bond observed in thiol-derived SAMs on coinage metal substrates.^{63,74} Both assignments

are discussed in detail in refs 45 and 75, but we would like to note here that in most situations, including the present case, the “different thiolate” assignment can be favored. We note also that when performing synchrotron-based HRXPS, we have frequently observed the doublet at 161.0 eV for different thiol-derived SAMs on both Au(111) and Ag(111) substrates.^{76,77} This doublet, even though very weak, is also present in the S 2p spectra of the **BPT** films as shown in Figure 3. All this indicates that such differently adsorbed sulfur seems to be a general phenomenon that needs further studies. A combination of HRXPS and scanning microscopic techniques can probably be quite useful in this regard.

3.3 Near Edge X-Ray Absorption Fine Structure Spectroscopy

Additional information about the identity, chemical composition, and fidelity of the films under consideration is provided by NEXAFS spectroscopy. This technique gives chemical information on the adsorbed species by sampling the electronic structure of their unoccupied molecular orbitals.⁷⁸ C *K*-edge spectra of the thiol- and thioether-based tripod ligand films acquired at an X-ray incidence angle of 55° are presented in Figure 4, along with the spectrum of a **BPT** film serving as reference (the spectra are not affected by possible linear dichroism effects at this particular experimental geometry). All spectra in Figure 4 exhibit an absorption edge related to excitations of the C 1s electrons into the continuum states and characteristic absorption resonances. The spectra are dominated by the pronounced π_1^* resonance of the benzene rings near 285.0 eV, which is accompanied by a Rydberg resonance (R^*) near 287.3 eV (this feature has also been associated with C–S moiety before) and several broad σ^* resonances at higher photon energies. The spectra of the **BPT** and **BPTT** SAMs exhibit an additional well-resolved π_2^* resonances near 288.8–288.9 eV, characteristic of non-disturbed benzene rings, underlining the high quality of these films (see the previous section). In the case of **PTT**, **PTET**, and **BPTET**, this feature is visible as only a weak shoulder of the peak near 288.5–286.6 eV assigned to the $\pi^*(C=O)$ resonance, which presumably stems from a contamination. The above assignments were made in accordance with refs 64 and 78–84.

The intensity of the characteristic π^* resonances should be representative of the film quality (the σ^* resonances are less suited for this purpose since they are less pronounced). On one hand, these resonances can be quenched to some extent upon a direct interaction of the phenyl moieties with metal substrate,⁷⁸ which does not occur in densely packed SAMs (upright orientation of the molecules) but can take place (to some extent) in disordered films. On the other hand, the resonance intensity can be expected to depend on the relative percentage of the ligand's benzene ring carbon atoms, because the NEXAFS spectra are normalized to the height of the C 1s absorption edge and, thus, to the total number of carbon atoms, viz. the carbon atoms from the benzene rings plus the SiCH₂S/SCH₃ carbon atoms from the binding units plus any carbon atoms associated with contamination that is always present in low-quality films. The respective percentages for the molecules studied here are reported in Table 3, where the observed intensities of the π_1^* resonance are also given. After correction of these intensities for the portion of the benzene ring carbon atoms, very similar values are observed for the **BPT**, **PTT**, and **BPTT** SAMs, with even higher values for the two latter systems (Table 3), which can be tentatively explained by excitonic and packing density effects.^{64,85,86} In contrast, the spectra of both thioether-based films (**PTET** and **BPTET**) exhibit very low intensities of the π_1^* resonance, both directly measured (Figure 4; Table 3) and corrected for the portion of the benzene ring carbon atoms (Table 3). This phenomenon can only be explained by a poor quality of the latter films in terms of low packing density, molecular disorder, and the presence of contamination.^{60–62}

Angle-dependent NEXAFS spectra, which can provide an insight into the average orientation of adsorbed species, were also acquired for the tripod ligand films and showed almost no linear dichroism in contrast to the reference **BPT** SAM. On one hand, this can

mean that the degree of orientational order in the former films was relatively low compared to the highly-ordered **BPT** SAM; this assumption is probably applicable to the **PTET** and **BPTET** films exhibiting characteristic signatures of structural inhomogeneity such as the comparably large FWHM of the main C 1s emission for **PTET** (see Figure 2) and low intensity of the characteristic π^* resonances due to quenching effects and a low number of precursor molecules present in the film for **PTET** and **BPTET** (see Figure 4 and Table 3). On the other hand, this can mean that the average value of molecular inclination in the tripod ligand films is close to the magic angle,⁷⁸ which can be expected for the **PTT** and especially for **BPTT** SAMs in view of the available XPS and NEXAFS data discussed above and, in more detail, below.

4. Discussion

According to the presented XPS and NEXAFS data, all the tripod ligands discussed in this work form monolayers on gold surfaces that are bound to the substrate via sulfur–gold bonds. Along with this general behavior, the thiol-based tripod ligands **PTT** and **BPTT** assemble into better defined and overall higher quality SAMs with improved film uniformity and chemical integrity compared to their thioether analogues **PTET** and **BPTET**.

We define quality in the current study to mean that the films are well defined both chemically and physically. Generally, the quality of a SAM is evaluated in terms of three factors: the packing density and alignment of the molecular backbones, the robustness and uniformity of the binding to the substrate, and the presence of contaminations in the film, with the latter factor being strongly dependent on the former two parameters. We will now discuss the SAMs of this study in regard to these three aspects.

The packing density of the **BPTET** SAM is significantly lower than that of the analogous thiol-based **BPTT** film. This is evident from the effective film thicknesses derived from the I_{C1s}/I_{Au4f} XPS intensity ratios, with the thioether system showing significantly lower values (10.0 Å and 12.0 Å for **BPTET** and **BPTT** films, respectively; see Table 1). The **PTET** film has also a higher film thickness (11.9 Å) as compared to the analogous thiol-based **PTT** layer (10.4 Å) but this is likely related to contamination on the gold surface and in the SAM matrix as evidenced by the respective XPS C 1s spectrum in Figure 2.

The degree of molecular alignment and order in the films can be tentatively evaluated on the basis of two parameters, the FWHM of the XPS C 1s emission and the intensity of the π_1^* C K-edge NEXAFS resonance. The width of the main XPS C 1s emission is noticeably narrower for the films formed by the thiol-based tripod ligands. This is of particular significance because these films have been measured using a laboratory XPS system, which has a slightly lower energy resolution than the synchrotron-based spectrometer used for the acquisition of the HRXPS spectra of thioether SAMs (~400 meV vs. ~100 meV). In part, this can be explained by the different percentage of the benzene ring and SiCH₂S/SCH₃ carbon atoms in the respective molecules since aromatic and aliphatic species have slightly different BEs, which can lead to a broadening of the joint emission line (due to electrostatic effects, such a line cannot, however, be considered as a simple superposition of the respective spectral contributions). On the other hand, **BPTET** and **PTT** have the same percentage of benzene ring carbon atoms but the C 1s emission from the films comprised of the thiol-based ligand (**PTT**) is significantly narrower. It is well established that a broadening of the C 1s emission can be associated with a lower packing density and higher heterogeneity in the target SAM.⁸⁶ This means that the thiol-based tripod ligands might have a better molecular alignment in the respective SAMs as compared to their thioether-based counterparts. This finding is in line with the analysis of the π_1^* NEXAFS resonance. As mentioned in the previous section, a strong π_1^* resonance is expected for homogenous

films, whereas disordered layers often show a diminished π_1^* signal. Both thioether tripod films exhibit disproportionately low intensities of the π_1^* resonances, which can only be explained by a high chemical and structural inhomogeneity in the thioether films compared to the thiol-based SAMs. It is important to note that, with respect to the portion of the benzene ring carbon atoms, the intensities of the π_1^* resonances for the thiol-based tripod ligand films (**PTT** and **BPTT**) are comparable to that for the monodentate **BPT** SAM, which has a high quality⁶⁰⁻⁶⁴.

The analysis of the XPS S 2p spectra of all the tripod ligand films suggests a superposition of several different bonding configurations in these systems in contrast to the reference **BPT** SAM, where the standard thiolate-type bonding dominates. Table 2 summarizes the relative intensities of the different sulfur species for the tripod ligand SAMs. The spectra of the thiol-based **PTT** and **BPTT** SAMs possess two different sulfur species, viz. thiolate (162.0 eV for S 2p_{3/2}) and unbound sulfur (163.2 eV) (for the latter sulfur species, both disulfide and unbound thiol groups are possible but unbound thiol seems to be more likely here). The former (bound) species accounts for 62.0 % and 54.9% of the total S 2p intensity, respectively. Since unbound species will in average be located closer to the SAM–ambient interface and, thus, their signal should be less attenuated by the hydrocarbon backbone, we can assume that the actual percentage of unbound sulfur atoms on the surface is slightly overrepresented in the spectra. Taking this effect into account, the fraction of thiolate-type sulfur is approaching 2/3, which suggests that, on the average, two out of three thiol anchors for each molecule are bonded to the substrate as a thiolate while the third one remains unbound. Conversely, the XPS S 2p spectra of the thioether-based films exhibit three different features characteristic of thioether (163.2 eV), “standard” thiolate anchor (162.0 eV), and the species at 161.0 eV. It is unclear at present to which extent the thioether species interact with the surface and whether they are involved in surface binding since the S 2p binding energies of unbound and weakly bound thioether moieties are almost identical in both scenarios. It is well established that thioethers can bind to the surface without C–S bond cleavage, and it is likely that a definite amount of thioether anchor groups will interact with the gold surface while the residual fraction will not be in contact with it. Even though the stoichiometry of the three different sulfur species in the **PTET** and **BPTET** films is not correlated to the three-fold symmetry of the tripodal binding unit, the combined fraction of the sulfur species strongly bound to the gold surface (the two thiolate species; doublets at 161.0 and 162.0 eV) account for nearly 2/3 of the total S 2p intensity, similar to the case of the thiol-based tripod ligands.

The observed coexistence of different sulfur species and a certain extent of inhomogeneous binding can be a general phenomenon for the molecules bearing tridentate headgroups with short-chain binding units and rigid spacer moieties, since uniform binding requires lateral assembly and molecular mobility. This is particularly true towards the end of the adsorption process when vacant adsorption sites on the surface can only accommodate a fraction of the binding units while the binding of the remaining units is sterically hindered. The respective extensive reorientation process at the surface after the initial binding has been observed for **PTET** and **BPTET** in a combined ellipsometry and optical second harmonic generation study.⁴⁵

Another specific feature of SAMs comprised of molecules bearing tridentate headgroups is a more important role of the headgroups in the structure-determining balance between the headgroup–substrate and intermolecular interactions. Whereas the van der Waals dimensions (cross-sections) of the molecular backbones are an important factor for packing density in the case of monodentate binding configuration, their importance diminishes likely in the case of tridentate headgroups, and sterical constraints at the SAM–substrate interface become a deciding factor, governing the packing density and molecular arrangement in the

SAM. This can lead to a partial disordering of the molecular backbones as compared to the monodentate system, where this ordering results from the backbone–backbone interaction of the neighboring molecules. This can probably explain the lack of the linear dichroism in the NEXAFS spectra of **BPTT** and **PTT**, in addition to the “magic angle” orientation hypothesis.

The latter system is of particular interest since the quality of the **PTT** film is surprisingly high compared not only to the film of the thioether counterpart (**PTET**) but even to monodentate benzenethiol (C_6H_5SH) SAMs on gold reported in the literature.⁶⁴ This deserves a special consideration. The molecular organization in SAMs of the monodentate benzenethiol is not yet fully understood and while ordered films with upright^{88·89} or strongly inclined⁹⁰ molecules have been reported, the majority of publications reports disordered and poorly defined films on gold.^{60·62·64} In particular, XPS and NEXAFS studies have shown a very heterogeneous binding behavior, oxygen-containing contaminations, and poor molecular alignment.⁶⁴ In contrast, according to the C 1s XPS spectra, the **PTT** film is almost free of contaminations (but probably contains some amount of physisorbed **PTT** species as follows from the comparison of the experimental and theoretical thickness values; see Table 1). Further, the pronounced π_1^* resonance related to the aromatic backbone is twice as intense in NEXAFS spectra of the **PTT** film as compared to the published spectra of benzenethiol on gold⁶⁴ and even comparable to that in the spectrum of the **BPT** SAM (see Figure 4 and Table 2).

The higher quality of the **PTT** film as compared to the monodentate analogue (benzenethiol SAM) can be probably explained by the role of the headgroup–headgroup interactions in the balance of structure-building forces in the tridentate case as discussed above. Whereas the dominant phenyl–phenyl interaction is probably not strong enough to achieve high film quality in the case of benzenethiol films on gold, the enhancement of the structure-building factor at the headgroup–substrate interface, as in the tridentate case, provides the desired quality improvement.

5. Conclusions

We have prepared and characterized SAMs formed on Au(111) by tripodal ligands with a phenyl or 4-biphenyl backbone and either thioether (**PTET** and **BPTET**) or thiol (**PTT** and **BPTT**) headgroups. The primary goal was the comparison of these tripodal systems in terms of the packing density, presence of contamination, homogeneity of the bonding configurations at the SAM–substrate interface, and overall quality of the respective films. XPS data suggest a better orientational order, higher packing density, and more uniform binding configuration for the thiol-based ligands as compared to their thioether counterparts. This finding is in line with the C *K*-edge NEXAFS data, which also imply a noticeably higher quality of the thiol-based tripod ligand films as compared to the thioether ones. In addition, a significantly lower amount of contamination was found in the thiol-based tripod ligand films, which can be primarily attributed to the self-cleaning effect upon the formation of densely packed SAM-like films.

The results obtained in this study suggest that the rational design of tridentate anchors can overcome steric effects of bulky tail groups and be a viable route for the assembly of phenyl-based SAMs on coinage metal substrates. In particular, the thiol-based tripod ligand **PTT** in this study yielded SAMs of significantly higher quality compared to its monodentate analogue, benzenethiol.

Inhomogeneity of the bonding configuration at the SAM–substrate interface was observed for all tripod ligand films of this study and appears to be an intrinsic property of these

systems. One cannot exclude, however, that this problem can be overcome by further improvement in the molecular design. Another interesting aspect is the headgroup–headgroup interaction in tripodal systems as a new factor for the competing structure-building forces in SAMs. This gives one an additional tool for adjusting SAM properties. In this regard, organosilicon chemistry could provide an efficient toolbox for the rational design of novel tridentate ligands for the fabrication of high-quality SAMs.

We hope that this study will stimulate further investigations of thiol-based tripodal ligands for the fabrication of SAMs. Scanning probe techniques would be particularly valuable for a closer look at the molecular organization in these films.

Supplementary Material

Refer to Web version on PubMed Central for supplementary material.

Acknowledgments

T. W., N. B., and M. Z. thank M. Grunze for the support of this work, C. Wöll and A. Nefedov for technical cooperation at BESSY II, L. S. O. Johansson (Karlstad University) for the cooperation at MAX-lab, and the BESSY II and MAX-lab staff for the assistance during the NEXAFS and HRXPS experiments. R. T. and D. T. thank C. Burschka for performing the crystal structure analysis. This work has been supported by German BMBF (05KS4VHA/4), DFG (ZH 63/9-3), and the European Community through the IA-SFS project within the Sixth Framework Programme. T. W. and D. G. C. thank NIH grant EB-002021 for support. T. W. thanks the German Research Foundation (DFG) for a research fellowship.

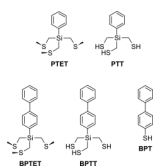
References

1. Ulman, A. *An Introduction to Ultrathin Organic Films*. Academic Press; San Diego: 1991.
2. Ulman, A. *Self-Assembled Monolayers of Thiols*. In: Ulman, A., editor. *Thin Films*, Vol. 24. Vol. 24. Academic Press; San Diego: 1998.
3. Schreiber F. *Prog. Surf. Sci.* 2000; 65:151–256.
4. Ulman A. *Acc. Chem. Res.* 2001; 34:855–863. [PubMed: 11714257]
5. Tour JM. *Acc. Chem. Res.* 2000; 33:791–804. [PubMed: 11087316]
6. Wohltjen H, Snow AW. *Anal. Chem.* 1998; 70:2856–2859.
7. Hickman JJ, Ofer D, Laibinis PE, Whitesides GM, Wrighton MS. *Science.* 1991; 252:688–691. [PubMed: 17746667]
8. Ratner BD, Bryant SJ. *Ann. Rev. Biomed. Eng.* 2004; 6:41–75. [PubMed: 15255762]
9. Castner DG, Ratner BD. *Surf. Sci.* 2002; 500:28–60.
10. Love JC, Estroff LA, Kriebel JK, Nuzzo RG, Whitesides GM. *Chem. Rev.* 2005; 105:1103–1169. [PubMed: 15826011]
11. Ferri V, Elbing M, Pace G, Dickey MD, Zharnikov M, Samori P, Mayor M, Rampi MA. *Angew. Chem.* 2008; 120:3455–3457. *Angew. Chem. Int. Ed.* 2008; 47:3407–3409.
12. Liu ZF, Hashimoto K, Fujishima A. *Nature.* 1990; 347:658–660.
13. Ikeda T, Tsutsumi O. *Science.* 1995; 268:1873–1875. [PubMed: 17797528]
14. Marten J, Erbe A, Critchley K, Bramble JP, Weber E, Evans SD. *Langmuir.* 2008; 24:2479–2486. [PubMed: 18257591]
15. Tour, JM. *Molecular Electronics: Commercial Insights, Chemistry, Devices, Architecture and Programming*. World Scientific; Singapore: 2003.
16. Kim K, Jeon WS, Kang J-K, Lee JW, Jon SY, Kim T, Kim K. *Angew. Chem.* 2003; 115:2395–2398. *Angew. Chem. Int. Ed.* 2003; 42:2293–2296.
17. Saha S, Johansson LE, Flood AH, Tseng HR, Zink JI, Stoddart JF. *Small.* 2005; 1:87–90. [PubMed: 17193355]
18. Yu Y, Nakano M, Ikeda T. *Nature.* 2003; 425:145. [PubMed: 12968169]

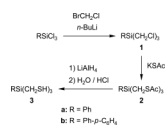
19. Hugel T, Holland NB, Cattani A, Moroder L, Seitz M, Gaub HE. *Science*. 2002; 296:1103–1106. [PubMed: 12004125]
20. Baisch B, Raffa D, Jung U, Magnussen OM, Nicolas C, Lacour J, Kubitschke J, Herges R. *J. Am. Chem. Soc.* 2008; 131:442–443. [PubMed: 19113847]
21. Whitesell JK, Chang HK. *Science*. 1993; 261:73–76. [PubMed: 17750549]
22. Park J-S, Vo AN, Barriet D, Shon YS, Lee TR. *Langmuir*. 2005; 21:2902–2911. [PubMed: 15779965]
23. Zhu L, Tang H, Harima Y, Yamashita K, Aso Y, Otsubo T. *J. Mat. Chem.* 2002; 12:2250–2254.
24. Hirayama D, Takimiya K, Aso Y, Otsubo T, Hasobe T, Yamada H, Imahori H, Fukuzumi S, Sakata Y. *J. Am. Chem. Soc.* 2002; 124:532–533. [PubMed: 11804479]
25. Kittredge KW, Minton MA, Fox MA, Whitesell JK. *Helv. Chim. Acta.* 2002; 85:788–798.
26. Schönherr H, Vancso GJ, Huisman B-H, van Veggel FCJM, Reinhoudt DN. *Langmuir*. 1999; 15:5541–5546.
27. Huisman B-H, Rudkevich DM, van Veggel FCJM, Reinhoudt DN. *J. Am. Chem. Soc.* 1996; 118:3523–3524.
28. Huisman B-H, Thoden van Velzen EU, van Veggel FCJM, Engbersen JFJ, Reinhoudt DN. *Tetrahedron Lett.* 1995; 36:3273–3276.
29. Thoden van Velzen EU, Engbersen JFJ, Reinhoudt DN. *J. Am. Chem. Soc.* 1994; 116:3597–3598.
30. Beulen MWJ, Bugler J, Lammerink B, Geurts FAJ, Biemond EMEF, van Leerdam KGC, van Veggel FCJM, Engbersen JFJ, Reinhoudt DN. *Langmuir*. 1998; 14:6424–6429.
31. Zobbi L, Mannini M, Pacchioni M, Chastanet G, Bonacchi D, Zanardi C, Biagi R, Del Pennino U, Gatteschi D, Cornia A, Sessoli R. *Chem. Commun.* 2005:1640–1642.
32. Weidner T, vor der Brüggen J, Siemeling U, Träger F. *Appl. Phys. B.* 2003; 77:31–35.
33. Hubenthal F, Borg N, Weidner T, Siemeling U, Träger F. *Appl. Phys. A.* 2009; 94:11–17.
34. Weidner T, Ballav N, Zharnikov M, Priebe A, Long NJ, Maurer J, Winter R, Rothenberger A, Fenske D, Rother D, Bruhn C, Fink H, Siemeling U. *Chem Eur. J.* 2008; 14:4346–4360.
35. Siemeling U, Rother D, Bruhn C, Fink H, Weidner T, Träger F, Rothenberger A, Fenske D, Priebe A, Maurer J, Winter R. *J. Am. Chem. Soc.* 2005; 127:1102–1103. [PubMed: 15669840]
36. Katano S, Kim Y, Kitagawa T, Kawai M. *Jpn. J. Appl. Phys.* 2008; 47:6156–6159.
37. Katano S, Kim Y, Matsubara H, Kitagawa T, Kawai M. *J. Am. Chem. Soc.* 2007; 129:2511–2515. [PubMed: 17279745]
38. Hu J, Mattern DL. *J. Org. Chem.* 2000; 65:2277–2281. [PubMed: 10789435]
39. Weidner T, Brethauer F, Ballav N, Motschmann H, Orendi H, Bruhn C, Siemeling U, Zharnikov M. *Langmuir*. 2008; 24:11691–11700. [PubMed: 18823085]
40. Zarwell S, Rück-Braun K. *Tetrahedron Lett.* 2008; 49:4020–4025.
41. Takamatsu D, Yamakoshi Y, Fukui K. *J. Phys. Chem. B.* 2006; 110:1968–1970. [PubMed: 16471770]
42. Sun F, Castner DG, Mao G, Wang P, McKeown P, Grainger DW. *J. Am. Chem. Soc.* 1996; 118:1856–1866.
43. Tsao M-W, Pfeifer K-H, Rabolt JF, Castner DG, Haussling L, Ringsdorf H. *Macromolecules.* 1997; 30:5913–5919.
44. Lavrich DJ, Wetterer SM, Bernasek SL, Scoles G. *J. Phys. Chem. B.* 1998; 102:3456–3465.
45. Weidner T, Krämer A, Bruhn C, Zharnikov M, Shaporenko A, Siemeling U, Träger F. *Dalton Trans.* 2006:2767–2777. [PubMed: 16751884]
46. Heister K, Zharnikov M, Grunze M, Johansson LSO. *J. Phys. Chem. B.* 2001; 105:4058–4061.
47. Moulder, JF.; Stickle, WF.; Sobol, PE.; Bomben, KD. *Handbook of X-ray Photoelectron Spectroscopy*. Perkin-Elmer Corp.; Eden Prairie: 1992.
48. Batson PE. *Phys. Rev. B.* 1993; 48:2608.
49. Apfel, U-P.; Troegel, D.; Halpin, Y.; Uhlemann, U.; Schmitt, M.; Popp, J.; Görls, H.; Dunne, P.; Venkatesan, M.; Coey, M.; Vos, JG.; Tacke, R.; Weigand, W. Manuscript in preparation
50. Troegel D, Walter T, Burschka C, Tacke R. *Organometallics.* 2009; 28:2756–2761.
51. Ilg R, Troegel D, Burschka C, Tacke R. *Organometallics.* 2006; 25:548–551.

52. Zefirov YV, Zorkii PM. *Zh. Strukt. Khim.* 1976; 17:745–746.
53. Dai J, Munakata M, Wu LP, KurodaSowa T, Suenaga Y. *Inorg. Chim. Acta.* 1997; 258:65–69.
54. Bleiholder C, Gleiter R, Werz DB, Köppel H. *Inorg. Chem.* 2007; 46:2249–2260. [PubMed: 17311376]
55. Bleiholder C, Werz DB, Koppel H, Gleiter R. *J. Amer. Chem. Soc.* 2006; 128:2666–2674. [PubMed: 16492053]
56. Mundt O, Becker G, Baumgarten J, Riffel H, Simon A. *Z. Anorg. Allg. Chem.* 2006; 632:1687–1709.
57. Ozturk T, Povey DC, Wallis JD. *Phosphorus, Sulfur, Silicon Relat. Elem.* 1997; 122:313–324.
58. Nagy P, Szabó D, Kapovits I, Kucsman A, Argay G, Kálmán A. *J. Mol. Struct.* 2002; 606:61–76.
59. Berg JM, Spira DJ, Hodgson KO, Bruce AE, Miller KF, Corbin JL, Stiefel EI. *Inorg. Chem.* 1984; 23:3412–3418.
60. Sabatani E, Cohen-Boulakia J, Bruening M, Rubinstein I. *Langmuir.* 1993; 9:2974–2981.
61. Dhirani A-A, Zehner RW, Hsung RP, Guyot-Sionnest P, Sita LR. *J. Am. Chem. Soc.* 1996; 118:3319–3320.
62. Tao Y-T, Wu C-C, Eu J-Y, Lin W-L, Wu K-C, Chen C. *Langmuir.* 1997; 13:4018–4023.
63. Ishida T, Choi N, Mizutani W, Tokumoto H, Kojima I, Azehara H, Hokari H, Akiba U, Fujihira M. *Langmuir.* 1999; 15:6799–6806.
64. Frey S, Stadler V, Heister K, Eck W, Zharnikov M, Grunze M, Zeysing B, Terfort A. *Langmuir.* 2001; 17:2408–2415.
65. Thome J, Himmelhaus M, Zharnikov M, Grunze M. *Langmuir.* 1998; 14:7435–7449.
66. Lamont CLA, Wilkes J. *Langmuir.* 1999; 15:2037–2042.
67. Castner DG, Hinds K, Grainger DW. *Langmuir.* 1996; 12:5083–5086.
68. Zhong C-J, Brush RC, Anderegg J, Porter MD. *Langmuir.* 1999; 15:518–525.
69. Trevor JL, Lykke KR, Pellin MJ, Hanley L. *Langmuir.* 1998; 14:1664–1673.
70. Beulen MWJ, Huisman B-H, van der Heijden PA, van Veggel FCJM, Simons MG, Biemond EMEF, de Lange PJ, Reinhoudt DN. *Langmuir.* 1996; 12:6170–6172.
71. Takiguchi H, Sato K, Ishida T, Abe K, Yase K, Tamada K. *Langmuir.* 2000; 16:1703–1710.
72. Kondoh H, Nozoye H. *J. Phys. Chem. B.* 1998; 102:2367–2372.
73. Yang YW, Fan LJ. *Langmuir.* 2002; 18:1157–1164.
74. Himmelhaus M, Gauss I, Buck M, Eisert F, Wöll C, Grunze M. *J. Electron. Spectrosc. Relat. Phenom.* 1998; 92:139–149.
75. Shaporenko A, Terfort A, Grunze M, Zharnikov M. *J. Electron. Spectrosc. Relat. Phenom.* 2006; 151:45–51.
76. Shaporenko A, Heister K, Ulman A, Grunze M, Zharnikov M. *J. Phys. Chem. B.* 2005; 109:4096–4103. [PubMed: 16851468]
77. Heister K, Rong H-T, Buck M, Zharnikov M, Grunze M, Johansson LSO. *J. Phys. Chem. B.* 2001; 105:6888–6894.
78. Stöhr, J. *NEXAFS Spectroscopy.* In: Ertl, G.; Gomer, R.; Mills, DL., editors. *Springer Series in Surface Sciences, Vol. 25.* Springer-Verlag; Berlin: 1992.
79. Weiss K, Bagus PS, Wöll C. *J. Chem. Phys.* 1999; 111:6834–6845.
80. Schöll A, Fink R, Umbach E, Mitchell GE, Urquhart SG, Ade H. *Chem. Phys. Lett.* 2003; 370:834–841.
81. Zharnikov M, Grunze M. *J. Phys.: Condens. Matter.* 2001; 13:11333–11365.
82. Fuxen C, Azzam W, Arnold R, Witte G, Terfort A, Wöll C. *Langmuir.* 2001; 17:3689–3695.
83. Paik MY, Krishnan S, You F, Li X, Hexemer A, Ando Y, Kang SH, Fischer DA, Kramer EJ, Ober CK. *Langmuir.* 2007; 23:5110–5119. [PubMed: 17397198]
84. Hitchcock AP, Fischer P, Gedanken A, Robin MB. *J. Phys. Chem.* 1987; 91:531–540.
85. Ågren H, Vahtras O, Carravetta V. *Chem. Phys.* 1995; 196:47–58.
86. Carravetta V, Ågren H, Pettersson LGM, Vahtras O. *J. Chem. Phys.* 1995; 102:5589–5597.
87. Heister K, Johansson LSO, Grunze M, Zharnikov M. *Surf. Sci.* 2003; 529:36–46.

88. Whelan CM, Barnes CJ, Walker CGH, Brown NMD. *Surf. Sci.* 1999; 425:195–211.
89. Carron KT, Hurley LG. *J. Phys. Chem.* 1991; 95:9979–9984.
90. Szafranski CA, Tanner W, Laibinis PE, Garrell RL. *Langmuir.* 1998; 14:3570–3579.

**Scheme 1.**

The structures of the tripod ligands addressed in this study (**PTT**, **BPTT**, **PTET**, and **BPTET**), along with the structure of the monodentate reference ligand **BPT**.



Scheme 2.
 Three-step synthesis of **PTT** and **BPTT**, starting from PhSiCl₃ and *p*-Ph-C₆H₄SiCl₃, respectively.

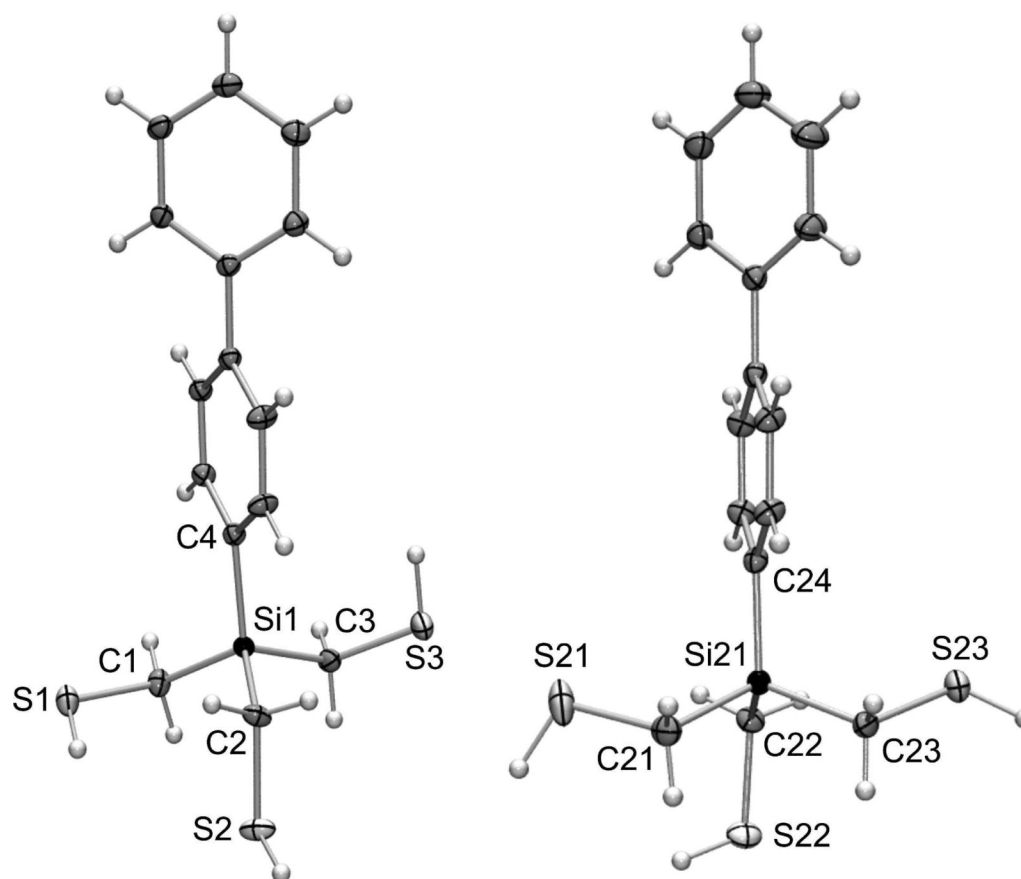


Figure 1.

Molecular structures of the two crystallographically independent molecules in the crystal of **BPTT** (probability level of displacement ellipsoids 50%). Selected bond lengths (Å) and angles (deg): Si1–C1 1.8784(11), Si1–C2 1.8745(11), Si1–C3 1.8691(11), Si1–C4 1.8667(11), S1–C1 1.8179(12), S2–C2 1.8182(12), S3–C3 1.8182(11); C1–Si1–C2 104.85(5), C1–Si1–C3 110.68(5), C1–Si1–C4 112.66(5), C2–Si1–C3 109.27(5), C2–Si1–C4 110.73(5), C3–Si1–C4 108.59(5), S1–C1–Si1 115.30(6), S2–C2–Si1 113.60(6), S3–C3–Si1 112.67(6); Si21–C21 1.8762(13), Si21–C22 1.8764(12), Si21–C23 1.8797(12), Si21–C24 1.8691(11), S21–C21 1.8189(14), S22–C22 1.8181(12), S23–C23 1.8129(13); C21–Si21–C22 110.59(6), C21–Si21–C23 106.39(6), C21–Si21–C24 110.59(5), C22–Si21–C23 109.07(5), C22–Si21–C24 109.60(5), C23–Si21–C24 110.55(5), S21–C21–Si21 110.01(7), S22–C22–Si21 111.03(6), S23–C23–Si21 111.18(6).

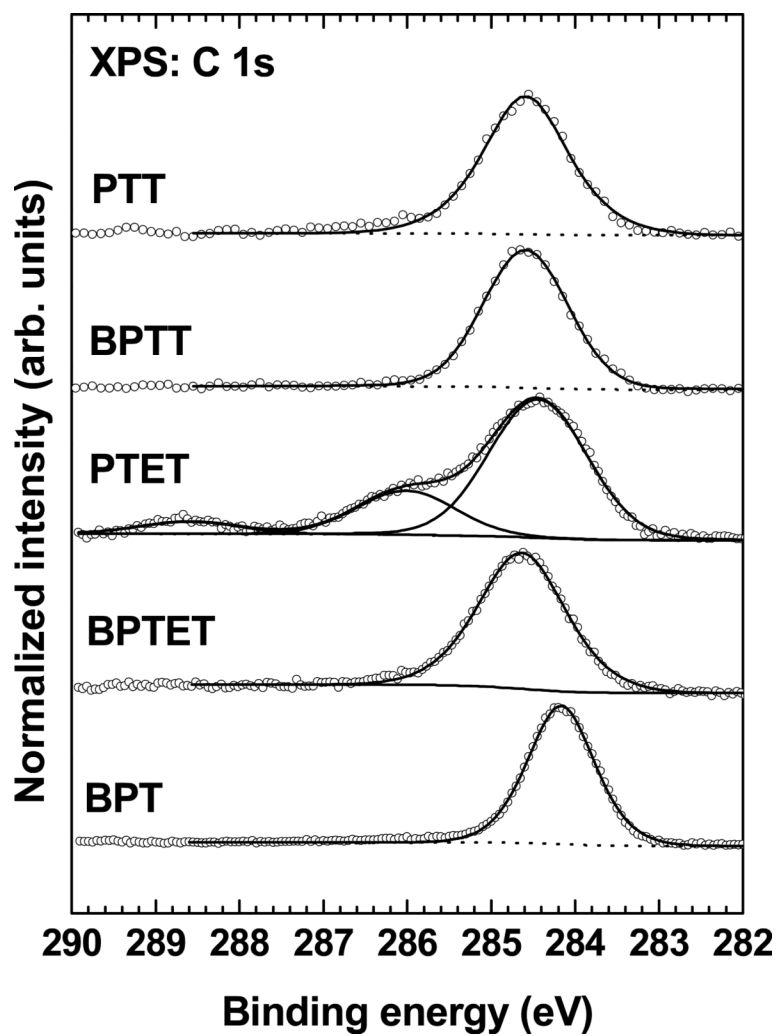


Figure 2. Normalized XPS C 1s spectra (open circles) of the **PTT**, **BPTT**, **PTET**, **BPTET**, and **BPT** SAMs on Au(111). The respective fits (solid lines), including the spectrum decomposition in the case of **PTET**, and a background (dotted line) are also shown.

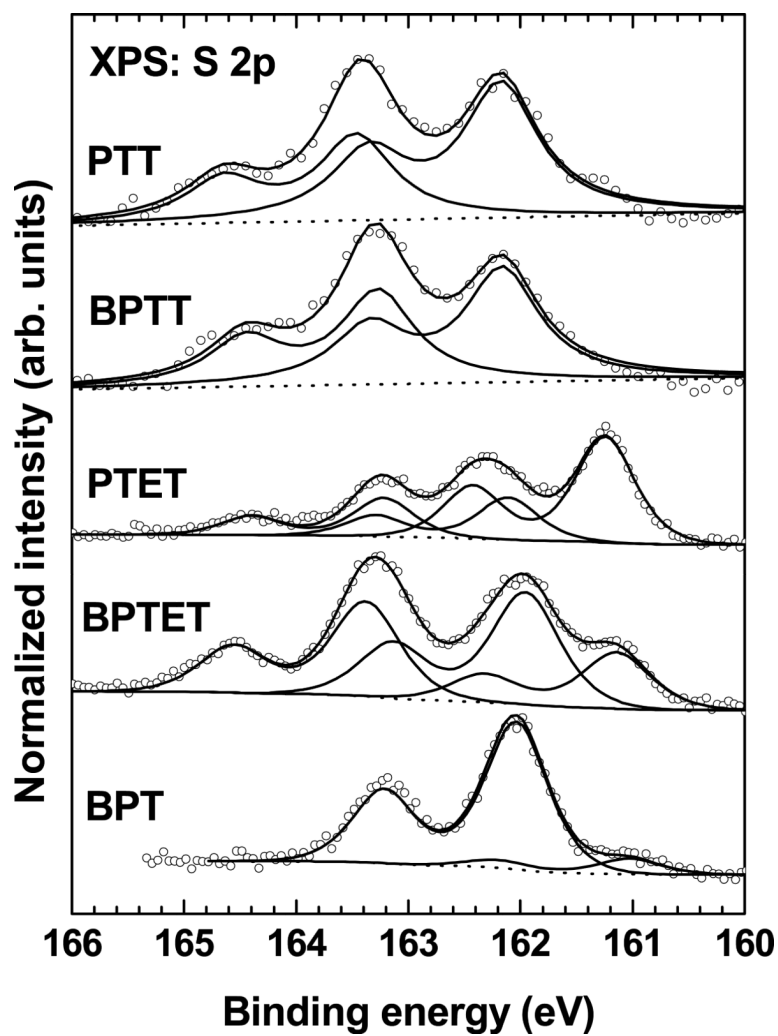


Figure 3. Normalized XPS S 2p spectra (open circles) of the **PTT**, **BPTT**, **PTET**, **BPTET**, and **BPT** SAMs on Au(111). The decomposition of these spectra into individual contributions (solid lines) and a background (dotted line) is also shown.

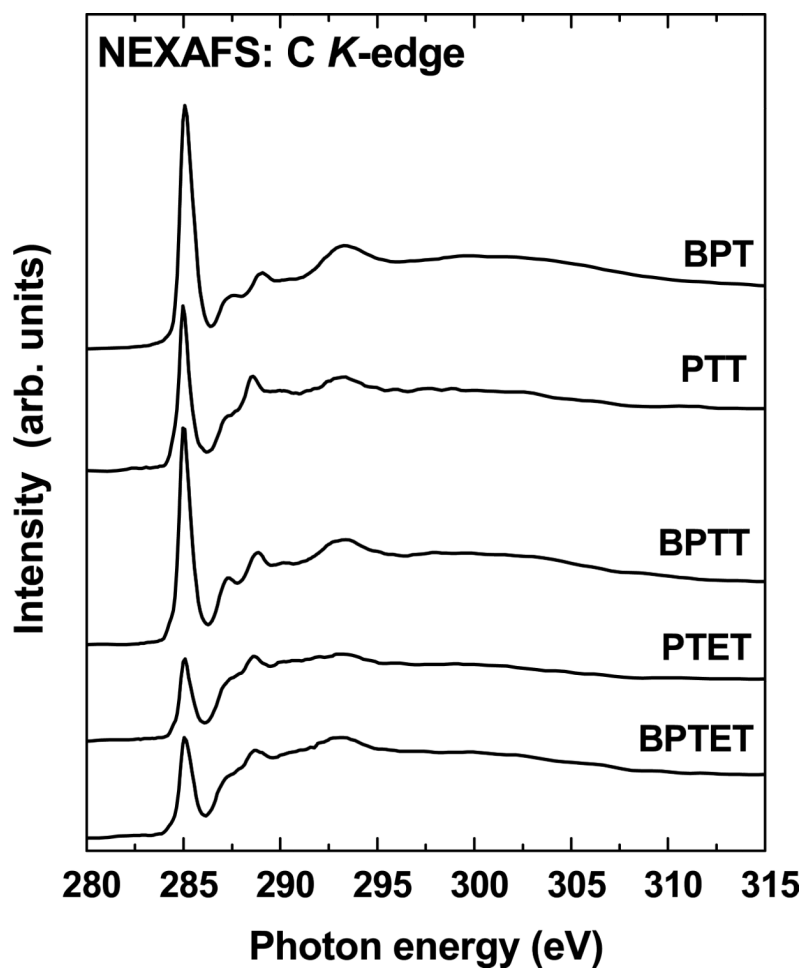


Figure 4. C *K*-edge NEXAFS spectra of the **BPT**, **PTT**, **BPTT**, **PTET**, and **BPTET** SAMs on Au(111) acquired at an X-ray incidence angle of 55°.

Table 1

Film thickness determined from the XPS data, along with the theoretical values for the thickness, which were calculated based on the molecular structure; a vertical orientation of the molecules in the films was assumed.

SAM	Film thickness / Å	Theoretical thickness / Å
PTT	10.4	9.1
BPTT	12.0	13.3
PTET	11.9	9.1
BPTET	10.0	13.3
BPT	11.7	12.7

Table 2

Relative intensities of the three characteristic doublets observed in the S 2p XPS spectra of the tripod ligand SAMs. The doublets can be assigned to the different sulfur species (see text for details).

Composition of S 2p emission (%)			
SAM	Thioether/unbound thiol (≈ 163.4 eV)	Thiolate (≈ 162 eV)	Low BE thiolate (≈ 161 eV)
PTT	38.0	62.0	-
BPTT	45.1	54.9	-
PTET	35.7	43.6	20.7
BPTET	36.0	42.6	21.4

Table 3

Comparison between the normalized intensity of the π_1^* resonance (with respect to the height of the absorption edge) in the C *K*-edge NEXAFS spectra of the target SAMs and portion of the benzene ring carbon atoms in the respective molecules (%). The ratio of both values, i. e., the normalized intensity of the π_1^* resonance corrected for the portion of the benzene ring carbon atoms in the respective molecules, is given in the third column.

SAM	π_1^* Intensity / a.u.	Portion of benzene ring carbon atoms (%)	π_1^* Intensity / a.u. (corrected for the portion of the benzene ring carbon atoms)
PTT	2.6	66	3.93
BPTT	3.3	80	4.125
PTET	1.2	50	2.4
BPTET	1.5	66	2.27
BPT	3.8	100	3.8